

1 **High-resolution automated detection of headwater streambeds for large watersheds**

2 **Francis Lessard<sup>1,2,3</sup>, Naïm Perreault<sup>1,2</sup>, Sylvain Jutras<sup>1,2,3</sup>**

3 <sup>1</sup> Department of Wood and Forest Science, Université Laval, 2405 rue de la Terrasse, G1V  
4 0A6, Québec, QC, Canada

5 <sup>2</sup> Centre d'étude de la forêt, Université Laval, 2405 rue de la Terrasse, G1V 0A6, Québec,  
6 QC, Canada

7 <sup>3</sup> CentrEau - Water Research Centre, Université Laval, 1065 avenue de la Médecine, G1V  
8 0A6, Québec, QC, Canada

9

10 **Corresponding author:** Francis Lessard, francis.lessard.3@ulaval.ca

11 **Present address:** Pavillon Abitibi-Price, 2405 rue de la Terrasse, G1V 0A6, Québec, QC,  
12 Canada

13

14 **Keywords:** LiDAR, Streambed, Headwater stream, Remote sensing

15       **Abstract:** Headwater streams, which are small streams at the top of a  
16 watershed, account for the majority of the total length of streams, yet their exact  
17 locations are still not well known. For years, many algorithms were used to  
18 produce hydrographic networks that represent headwater streams with varying  
19 degrees of accuracy. Although digital elevation models derived from LiDAR  
20 have significantly improved headwater stream detection, the performance of  
21 the algorithms on landscapes with different geomorphologic characteristics  
22 remains unclear. Here, we address this issue by testing different combinations  
23 of algorithms using classification trees. Homogeneous hydrological processes  
24 were identified through Quaternary deposits. The results showed that in  
25 shallow soil that mainly consists of till deposits, the use of algorithms that  
26 simulate the surface runoff process provide the best explanation for the  
27 presence of a streambed. In contrast, streambeds in thick soil with high  
28 infiltration rates were primarily explained by a small-scale incision algorithm.  
29 Furthermore, the use of an iterative process that simulate water diffusion made  
30 it possible to detect streambeds more accurately than all other methods tested,  
31 regardless of the hydrological classification. The method developed in this  
32 paper shows the importance of considering hydrological processes when  
33 aiming to identify headwater streams.

34       197 words

35

## 36    **1.    Introduction**

37 Streams are characterized by the presence of natural linear depressions, called streambeds.  
38 Streambeds, which are formed by fluvial processes, consist of a bed floor and banks, and  
39 are identified morphologically. The upstream location of a streambed is generally  
40 recognized as being the beginning of a stream and is referred as the channel head. At times,  
41 streambeds can be discontinuous or diffuse, leading to subjective identification of  
42 streambeds in the field and influence the determined location of the surveyed channel head  
43 (Dietrich and Dunne, 1993; Wohl, 2018). On a large scale, headwater streams are  
44 extremely important to maintain natural hydrological processes. Indeed, they are  
45 representing about two-thirds of the total length of streams in a large watershed (Leopold  
46 et al., 1964). Because they have varied ecosystems that include ecotones, headwater  
47 streams support rich and diverse fauna and flora (Meyer et al., 2007). In addition,  
48 headwater streams provide many ecological services to humans, including good quality  
49 drinking water (Alexander et al., 2007; Freeman et al., 2007) and flood control (St-Hilaire  
50 et al., 2016). Creed et al. (2017) estimated that for 2.9 million km of headwater streams in  
51 the United States, 15.7 trillion US \$ in ecological services are provided annually.

52 Cartographic information on headwater streams at national or provincial scales are largely  
53 derived from photointerpretation of stereoscopic aerial photography. This is the main  
54 method used for the Géobase du réseau hydrographique du Québec (GRHQ) in Quebec  
55 province, Canada. This geodatabase combines and standardizes several sources of  
56 hydrographic data, covering an area of 154 million hectares and representing millions of  
57 hydrographic features identified from aerial photos. Unfortunately, this database, as others  
58 such as NHD (National Hydrography Dataset), underestimates the true length of streams  
59 since photointerpretation methods are especially inaccurate when identifying where

60 streams begin and where they become perennial (Hafen et al., 2020). Streambeds are often  
61 imperceptible on stereoscopic images where only the wide valleys are evident  
62 (Montgomery and Dietrich, 1994).

63 Other methods based on a digital elevation model (DEM) have been used for several years  
64 to detect streams. These methods, used to produce hydrographic networks, can be divided  
65 into two main categories: channel initiation and valley recognition (Lindsay, 2006). The  
66 channel initiation method can be used to identify the potential locations of streambeds by  
67 thresholding a flow accumulation raster by a minimum drainage area (Band, 1986; Fairfield  
68 and Leymarie, 1991; Jenson and Dominique, 1988; O'Callaghan and Mark, 1984). Valley  
69 recognition can be used to detect streambeds locally through a moving window that  
70 identifies specific pattern depending on the algorithm used (Passalacqua et al., 2012;  
71 Peucker and Douglas, 1975; Tribe, 1992). Other authors have attempted to include the  
72 slope to a flow accumulation raster in order to produce more explicit models (Elmore et  
73 al., 2013; Henkle et al., 2011; James et al., 2010; Montgomery and Foufoula-Georgiou,  
74 1993). These methods have been widely used with coarse resolution DEMs (greater than  
75 10 m) that have generally been derived from aerial photos.

76 High resolution geospatial data from Light Detection and Ranging (LiDAR) technology  
77 allows for more accurate detection of headwater streams by providing topographic data on  
78 the microtopography under the forest canopy and allowing the creation of DEMs with  
79 unprecedented accuracy (Murphy et al., 2008; Wulder et al., 2008). The hydrographic  
80 networks generated with these new DEMs are much more accurate than those derived from  
81 photointerpretation or those produced from DEMs with a coarser resolution (Goulden et  
82 al., 2014). Various authors have attempted to use these DEMs to improve the accuracy of

83 hydrographic networks and the position of channel heads. LiDAR-derived DEMs have  
84 been used to detect streams both locally (Cho et al., 2011; James et al., 2007) and through  
85 channel initiation using a drainage area threshold (Murphy et al., 2008; Persendt and  
86 Gomez, 2016). While LiDAR-derived DEMs are more representative of the local impact  
87 of water, they still ignore the heterogeneity of Quaternary deposits that can affect  
88 streambed formation. Among other things, some authors noted the sensitivity of local flow  
89 direction to the elevation error of the DEM (Hengl et al., 2010; O’Neil and Shortridge,  
90 2013; Schwanghart and Heckmann, 2012). DEMs derived from LiDAR data were also used  
91 to quantify the variability of perennial stream flow lengths, although those studies did not  
92 specify where the streambed begins (Jensen et al., 2018, 2019; Van Meerveld et al., 2019).  
93 To the best of our knowledge, no study has addressed streambed detection using LiDAR  
94 data while considering both channel initiation and valley recognition methods (Heine et  
95 al., 2004) on a territory with heterogeneous geomorphologic characteristics, such as slope  
96 or Quaternary deposits (Wu et al., 2021). Also, no study uses such a large calibration  
97 database from real observations acquired in the field.

98 The main objective of this study is to detect headwater streambeds at a provincial scale.  
99 Specific objectives are to consider hydrological processes through Quaternary deposits and  
100 to use simple, well-documented streambed detection methods that can be exported to  
101 different geomorphologic contexts with local calibration data. The proposed method  
102 overcomes the many challenges that have limited efficient streambed detection in the past.  
103 These challenges include highly heterogeneous geomorphologic characteristics (such as  
104 Quaternary deposits) and strong anthropization of the land, as observed in numerous

105 agricultural watersheds where headwater streams have been straightened and deepened  
106 (Couture, 2023; Sanders et al., 2020).

## 107 2. Study areas

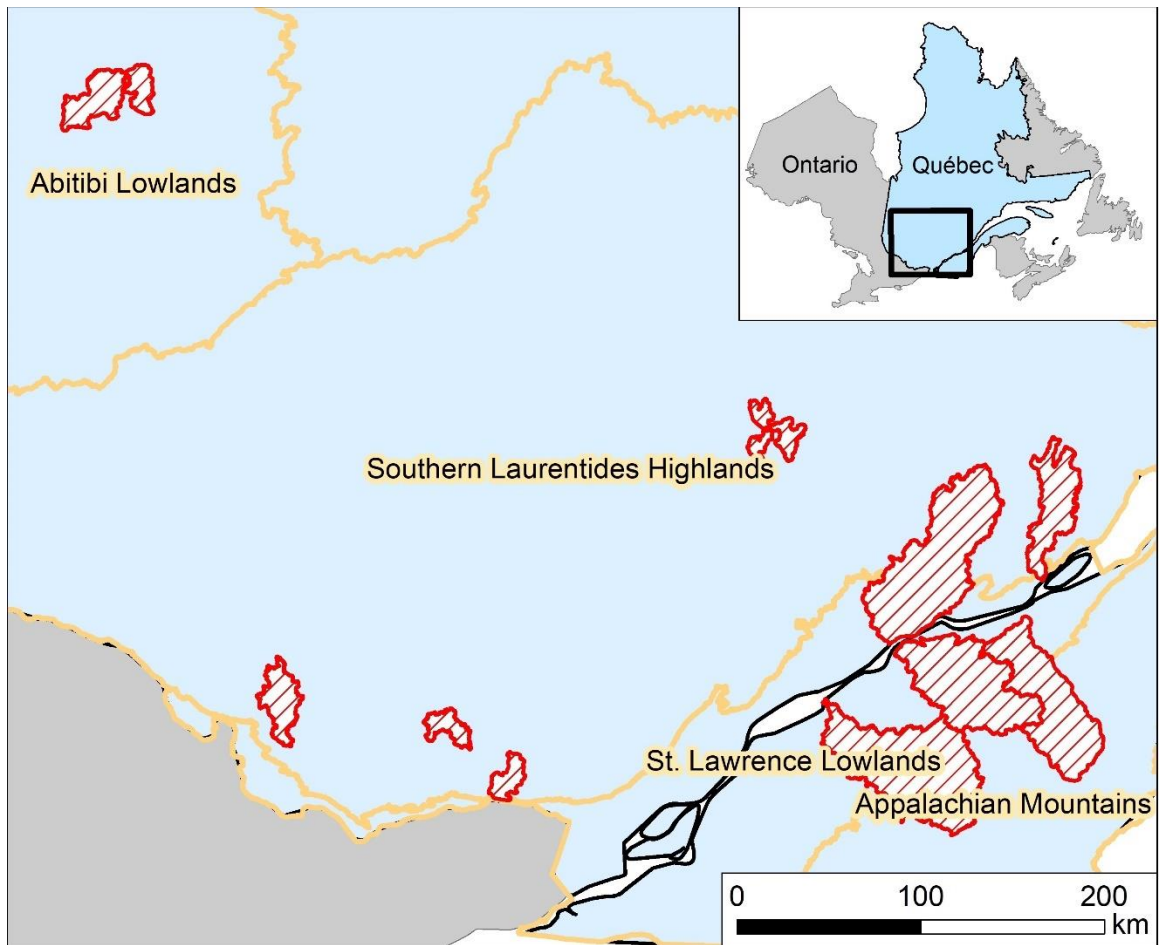
108 The study areas were located in the Appalachian Mountains, St. Lawrence Lowlands,  
109 Southern Laurentides Highlands and Abitibi Lowlands natural provinces, according to the  
110 Quebec Ecological Reference Framework (Fig. 1). This reference framework divides the  
111 territory of Quebec into spatially homogeneous units at various, intertwined levels. The  
112 different levels describe homogeneous units in terms of landform, spatial organization, and  
113 hydrographic network configuration (Direction de l'expertise en biodiversité, 2018). The  
114 diversity of the natural provinces thus selected provides a general representation of the  
115 headwater streams in Quebec. These natural provinces have distinct hydrological processes  
116 resulting from geological structure and Quaternary deposits.

117 The Southern Laurentides Highlands is mostly covered by till, the most widespread  
118 Quaternary deposit in the province of Quebec (Blouin and Berger, 2004; Gosselin, 2002).  
119 This natural province is mountainous, with altitudes varying from 200 to 1200 m. The  
120 bedrock mainly consists of gneiss. Quaternary deposits are generally thin on summits and  
121 steep slopes and thicker on valley bottoms and gentle slopes. The land in the Southern  
122 Laurentides Highlands is largely forested. In the Appalachian Mountains, the Quaternary  
123 deposits are somewhat similar in distribution to those in the Southern Laurentides  
124 Highlands, although they are thicker in certain areas. However, the bedrock in the  
125 Appalachian Mountains is sedimentary and therefore very different from the Southern  
126 Laurentides Highlands. The altitude here varies from 0 to 1200 m. Unlike the Southern  
127 Laurentides Highlands, there is high anthropization of this natural province due to  
128 agriculture (Gosselin, 2005a). In the St. Lawrence Lowlands, agricultural activity is also  
129 widespread. The Quaternary deposits in this region are highly heterogeneous and are

130 mainly derived from marine and glaciolacustrine geomorphologic processes. These  
131 processes lead to thick soils of sorted material, including clay and sand. These, in turn,  
132 create deposits that range from impermeable to very permeable. In addition to clay and  
133 sand, organic deposits are also present. The elevation of the St. Lawrence Lowlands is  
134 generally less than 100 m, as it was formed from the Champlain Sea during deglaciation  
135 (Gosselin, 2005b). In the Abitibi Lowlands, the Quaternary deposits are rather thick and  
136 consist of silt and clay. These deposits were produced by marine and lacustrine invasions  
137 and are conducive to the formation of large peatlands. Therefore, the area is relatively flat  
138 with altitudes varying from 0 to 350 m. Where present, the bedrock is made of basalt and  
139 gneiss (Blouin and Berger, 2002).

140 Precipitation is not seasonal, but rather constant throughout the year in all study areas.  
141 Precipitation amounts are quite homogeneous and range from 900 mm/year to 1100  
142 mm/year, except in Southern Laurentides Highlands where it can reach 1450 mm/year.  
143 Approximately 20 % of the precipitation falls as snow during the cold season, except in the  
144 coldest regions such as the Abitibi Lowlands and the higher altitude areas of the Southern  
145 Laurentides Highlands where the proportion of snow can reach 30%. Indeed, the average  
146 annual temperature of all the study areas is 3° C to 5° C, except for these two regions where  
147 it is 0° C (MELCC, 2022).





148

149 **Figure 1** : Study areas in the Appalachian Mountains, St. Lawrence Lowlands, Southern  
 150 Laurentides Highlands and Abitibi Lowlands natural provinces. Red polygons represent  
 151 watersheds where field surveys were carried out. [Color is not required for this figure.  
 152 **Single column fitting figure.**]

153

### 154 **3. Methods**

#### 155 *3.1. Field surveys*

156 Field based data collection is essential to fully understand stream flow patterns. Field  
 157 surveys were conducted from 2017 to 2021 during summer periods using an EOS GNSS  
 158 Arrow 100 sub-meter precision GPS. The horizontal accuracy of these devices is

159  $\pm 0.6$  m in open areas and  $\pm 1.2$  m in forested areas (Estrada, 2017). These devices were  
160 connected to rugged cell phones in order to use the ArcGIS Field Maps application to  
161 integrate data collection forms as well as relevant background maps.

162 The positions of streams were recorded from downstream at drainage area generally under  
163 1000 ha to upstream until the streambed completely disappeared. The flow regime, the  
164 width of the streambed, the extent of the water occupation in the streambed and the  
165 presence or the absence of a water flow were collected along the stream path to establish a  
166 high level of understanding. A position was taken on the streams every 50 m or so where  
167 a streambed was present, i.e. where the stream had a bed floor and banks formed by a  
168 fluvial process. Other positions were also taken to identify where there was no streambed.

169 This information was essential for consistent calibration and validation of streambeds.

170 To ensure consistent data collection, a 50 m x 50 m grid was used to determine which areas  
171 should be fully surveyed. These areas were mostly located at headwater streams to be able  
172 to include channel heads. This procedure was essential to properly assess the upstream  
173 boundary of the headwater streams and precisely record where the streambeds begin, where  
174 they flow from the watershed to the perennial stream, and where they are absent.

### 175 3.2. *Variables used for analysis*

176 The geomatic manipulations were mainly performed with the ArcGIS Desktop 10.7  
177 software package, including the Spatial Analyst and 3D Analysis extensions. The open-  
178 source SAGA-GIS (Conrad et al., 2015) and WhiteboxTools (Lindsay, 2016a) software  
179 were also used.

180 The variables used for analysis were produced from 1 m resolution DEMs of the different  
181 areas. These were generated from LiDAR data by the MFFP (Ministère des Forêts, de la

182 Faune et des Parcs), with a density of around 2.5 points/m<sup>2</sup>. LiDAR acquisitions were  
183 conducted from 2016 to 2019 (Leboeuf and Pomerleau, 2015), except for a few areas. The  
184 road network was carefully examined to include and burn all culverts that could affect the  
185 flow direction (Lessard et al., 2023). Indeed, hydrographic networks are greatly affected  
186 by deviations caused by the embankment of the roads. This type of anthropic influence  
187 must therefore be minimized to generate coherent flow direction (Li et al., 2013).  
188 Furthermore, the use of a breaching algorithm allowed to generate hydrologically coherent  
189 DEMs prior to hydrographic modeling (Lindsay, 2016b; Lindsay and Dhun, 2015).  
190 Physiographic factors must also be considered during the modeling process as they  
191 significantly influence the location of channel heads and the flow regime along streams.  
192 On the local scale, where the precipitation regime is uniform (Tucker and Slingerland,  
193 1996), slope, hydraulic force and sediment cohesion generally dictates streambed  
194 formation (Dietrich and Dunne, 1978). The influence of these factors is variable depending  
195 on the type of Quaternary deposit (Dietrich and Dunne, 1993; Dunne and Black, 1970;  
196 Montgomery and Dietrich, 1994).  
197 Quaternary deposits can be used to assess which processes are involved in the formation  
198 of a streambed. There are two major types of streambed formation processes. The first type  
199 involves surface processes, which occurs when soil that has low permeability is exposed  
200 to rainfall amounts that exceed the infiltration capacity of the ground, causing surface  
201 runoff (Horton, 1945). Then, when the power of the water exceeds the cohesion of the  
202 sediments, usually in concavities, a streambed forms (Dietrich and Dunne, 1978). The  
203 second type involves subsurface processes that occur when the Quaternary deposits are  
204 thick and infiltrative. Water vertically infiltrates into the ground and eventually reaches

205 saturation at a junction with the water table, the bedrock, or an inferior and less infiltrating  
206 deposit. Then, lateral movement of the groundwater occurs. Water emerges from the  
207 ground when there is a change in slope or soil permeability. Streambeds formed in this way  
208 tend to be heavily incised, with flow regimes that are more stable than those formed through  
209 surface processes. Thus, the hydrological response of the streams from subsurface  
210 processes is slightly affected by the intensity of rainfall (Dunne and Black, 1970; Jensen et  
211 al., 2019; Wohl, 2018). Furthermore, it should be noted that there is a gradient between  
212 these two processes for each stream. In order to properly detect streambeds, it is essential  
213 to distinguish these processes through hydrological classification according to Quaternary  
214 deposit type and land use.

215 Quaternary deposit mapping has been standardized across the province of Quebec and  
216 information was collected through photointerpretation conducted several years ago. Since  
217 photointerpretation was mainly used to distinguish forest structures and land use, the true  
218 boundaries of the Quaternary deposits are imprecise, in some cases. Quaternary deposit  
219 boundaries in agricultural areas are more accurate than those in forested areas because no  
220 other information was mapped during the process. Regardless of these drawbacks,  
221 standardized mapping provides a rough description of the nature and thickness of  
222 Quaternary deposits.

223 Spatially heterogeneous Quaternary deposits in Quebec have been classified into three  
224 categories and are described in Table 1 (Saucier et al., 1994). The purpose of this  
225 classification step is to differentiate the two types of hydrological processes for headwater  
226 stream formation that were previously described (Dietrich and Dunne, 1993; Lessard,  
227 2020). These classifications consider the infiltration capacity and the water storage

228 capacity of the ground (Dunne and Black, 1970). The two main variables considered were  
 229 the potential thickness and the granulometry of the Quaternary deposits (Dietrich and  
 230 Dunne, 1993; Wohl, 2018). Thus, the hydrological classes in Table 1 allow us to group  
 231 together streams whose formation is driven by similar, and therefore theoretically  
 232 homogeneous, hydrological processes.

233

234 **Table 1** : Hydrological classification according to Quaternary deposit types

Hydrological class	Quaternary deposits involved
Shallow soil	Glacial deposits without morphology such as till, frequent rock outcrops.
Thick soil with high infiltration rate	Glacial deposits with morphology such as moraines, glaciofluvial deposits, fluvial deposits, coarse lacustrine and marine deposits, slope deposits and eolian deposits; Agricultural land use, regardless of anthropic modifications due to straightening and deepening of streambeds, has been included in this class as agriculture is mainly carried out on the above deposits.
Thick soil with low infiltration rate	Lacustrine and fine marine deposits, organic deposits.

235

236 The first analysis variable, called ‘D8’, refers to the D8 flow accumulation (O’Callaghan  
237 and Mark, 1984) produced with a 1 m resolution DEM. This variable was selected as it is  
238 the most common algorithm used to produce hydrographic networks. For meaningful  
239 correspondence analysis between this variable and field surveyed streams, the flow  
240 accumulation raster was aggregated at 3 m resolution according to the maximum value.  
241 Then, a maximum focal statistic of two pixels was applied. The purpose of this treatment  
242 was to ensure a 6 m analysis distance between the D8 and the edge of a real stream,  
243 represented in the database by a vector line feature. This prevents the omission error from  
244 being overestimated.

245 The second analysis variable uses the D8 flow accumulation algorithm while considering  
246 flow direction error due to the elevation uncertainty of the LiDAR-derived DEM (Hengl et  
247 al., 2010; O’Callaghan and Mark, 1984). This variable, called ‘PROB’, quantifies the  
248 uncertainty associated with the position of the drainage network. This variable allows water  
249 diffusion processes to be simulated more adequately than the multiple flow direction  
250 algorithms that have been developed for this purpose (Freeman, 1991). Murphy et al.,  
251 (2009) noted a convergence of results between the single and multiple flow direction  
252 algorithms using high-resolution DEMs derived from LiDAR data. The use of a multiple  
253 direction algorithm did not provide better results for simulating soil moisture. Indeed, the  
254 dendritic flow pattern still appeared visible in the wetlands, even with the use of a multiple  
255 flow direction algorithm, probably due to the microtopography present in these DEMs. The  
256 elevation error in the DEM is directly related to the uncertainty of the LiDAR data  
257 (Wechsler, 2007) and impacts the position of the hydrographic network (Lindsay, 2006).  
258 This type of error is affected by the landform, and mainly occurs on gentle slopes and

259 slightly convex terrain (Hengl et al., 2010). Since this type of error is inherent to the shape  
260 of the land, it is not affected by the size of the drainage area implied. The iterative method  
261 described in Hengl et al. (2010) was reproduced in order to create the PROB variable. The  
262 method is based on repeatedly computing a flow accumulation raster from an initial DEM  
263 and several altered versions of the DEM. These altered versions are created by adding  
264 random elevation errors to the initial DEM to reproduce the elevation errors from the  
265 LiDAR data. As described by Richardson and Millard (2018) the typical ground return  
266 elevations errors therefore had a standard deviation of 0.08 m, randomly distributed over  
267 the DEM. A focal statistic of 3 m was used on the error raster to ensure the spatial  
268 autocorrelation of errors. Based on the convergence observed by Lindsay (2006), 50  
269 iterations were carried out. Then, each of the flow accumulation rasters were thresholded  
270 to a 1.5 ha drainage area to sum the resulting binary stream network, where a value of 1  
271 indicated the presence of a streambed and a 0 indicated the absence of a streambed. The  
272 matrix of the cumulative value was then normalized as a percentage to be used as an  
273 analysis variable. This PROB variable revealed the extent of the diffusion process of the  
274 water in in valley bottoms, small wetland or riparian areas, where the slope is relatively  
275 low or the topography slightly convex. The PROB variable was produced with a 3 m  
276 resolution DEM from a 1 m resolution DEM that was aggregated using the mean values.  
277 An average flow accumulation raster that corresponded to the average of the 50 flow  
278 accumulations raster without thresholding was also produced. This raster was used to create  
279 the analysis database and to calculate the drainage area of the channel heads. To ensure a  
280 6 m analysis distance as well as the D8 variable, a maximum focal statistic of two cells was  
281 performed before summing or averaging the iterated rasters.

282 The third variable used for analysis is morphometric and allows for the complementary  
283 detection of headwater streams (Lindsay, 2006; Tribe, 1992). The morphometric algorithm  
284 used was the topographic position index, referred to as 'TPI'. This algorithm allowed for  
285 the local detection of small incisions that might represent streambeds (Tribe, 1992). The  
286 scale at which this variable is calculated strongly influences the morphometric feature that  
287 is identified. When the scale is large, the variable will tend to identify valleys, while it  
288 tends towards streambeds when the scale is small (Montgomery and Dietrich, 1992, 1994).  
289 For the purposes of this paper, a relatively small scale of 6 to 30 m was used. This scale is  
290 consistent with the width of the majority of inventoried streambeds. The DEM used to  
291 calculate this variable had a resolution of 2 m and was derived from aggregating a 1 m  
292 resolution DEM with the minimum values. The tool named 'Topographic Position Index'  
293 in SAGA-GIS software was used to produce this variable (Guisan et al., 1999; Weiss,  
294 2001). The TPI variable has not been normalized to allow comparison of the values  
295 between the different study areas.

### 296 *3.3. Analysis database*

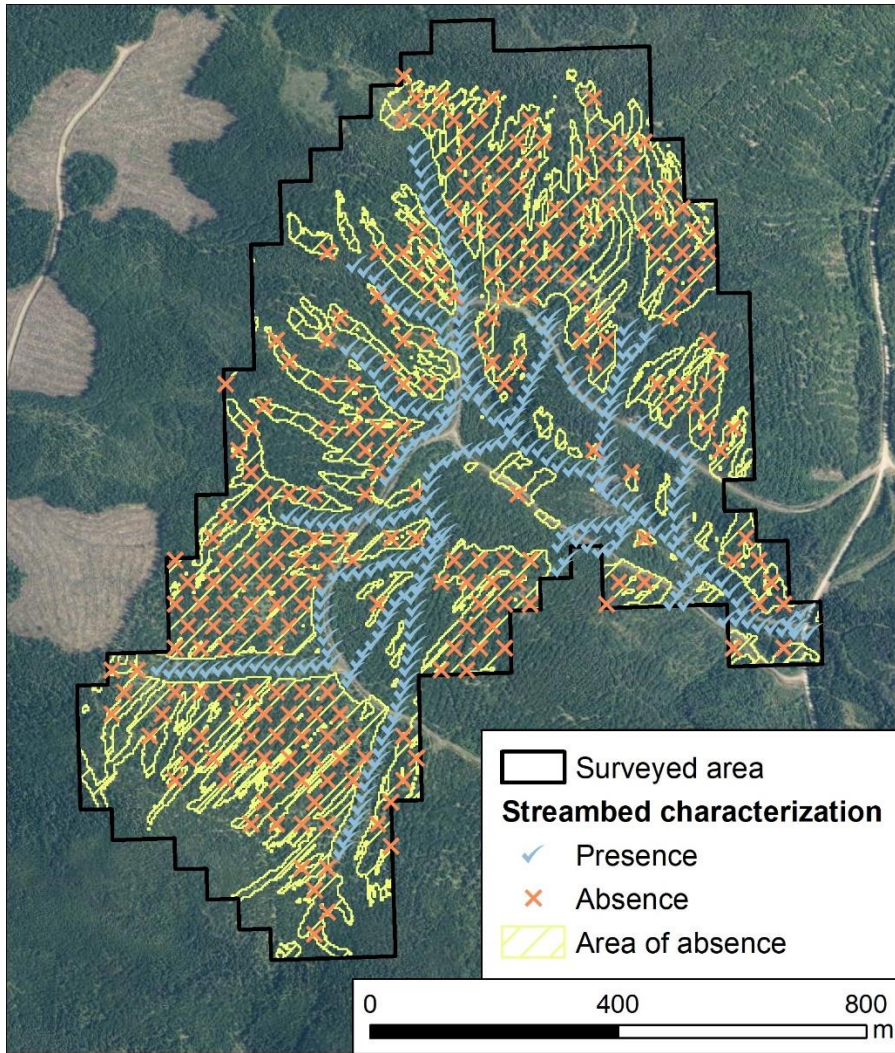
297 In order to perform the subsequent analyses, all actual streambeds were vectorized and geo-  
298 interpreted according to the stream positions recorded in the field. It should be noted that  
299 information on the flow regime was not used in this database. Instead, the presence of a  
300 streambed was used to describe the presence or absence of a stream. Although some  
301 streambeds have been straightened and deepened, particularly in anthropic lands,  
302 streambed was considered to be present only when natural fluvial processes allow it to be  
303 maintained. The presence of geo-interpreted vector lines features indicated the exact  
304 location of the streambeds and were complemented by a 50 m x 50 m grid to represent the



305 complete surveyed area. Thus, areas without a vector line feature have been assumed as  
306 not containing streambeds.

307 Positions representing the presence of streambeds were systematically located every 20 m  
308 along vector lines features that described real streams. Then, positions representing the  
309 absence of a streambed were located according to a sampling principle based on minimum  
310 flow accumulation where it was still coherent to observe the presence of a streambed. First,  
311 within the grid of the surveyed area, the average flow accumulation raster was thresholded  
312 at 0.11 ha. This threshold represents the lowest drainage area for initiation of channel head  
313 according to Lessard (2020). Then, the resulting raster was converted to a polygon.  
314 Following that step, a 20 m buffer zone was removed around the vector lines features that  
315 represent real streams. Thus, polygons identifying absence positions were located only in  
316 areas with a minimum of 0.11 ha mean drainage area and a minimum distance of 20 m  
317 from any real streams. Finally, absence positions were systematically located according to  
318 a hexagonal distribution in the final resulting polygon. The number of absence positions  
319 was equalized with the number of presence positions for each natural region within the  
320 Quebec ecological reference framework.

321 The analysis database was therefore composed of positions describing both the presence  
322 and the absence of streambeds (Fig. 2). The values for the three variables described in the  
323 previous section (D8, PROB and TPI) were extracted for all presence and absence  
324 positions.



326 **Figure 2** : Analysis database of positions indicating the presence and absence of  
 327 streambeds (Aerial images from continuous imagery of the Government of Quebec;  
 328 MRNF). [Color is not required for this figure. Single column fitting figure.]

329

330 *3.4. Statistical analysis*

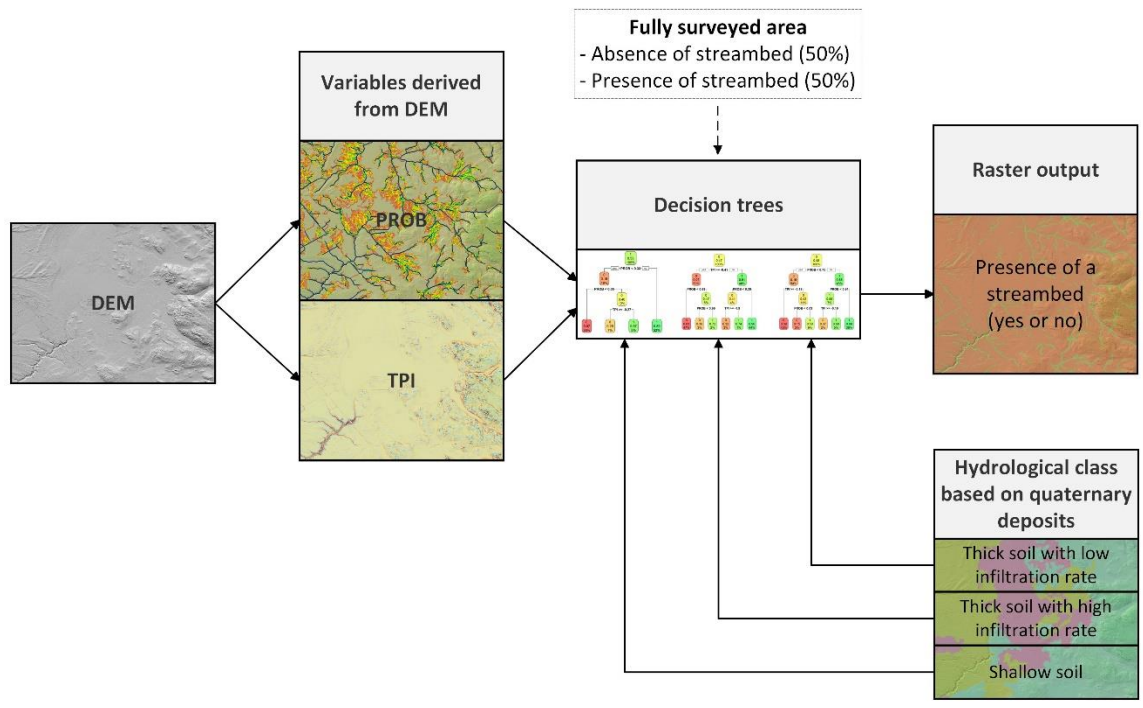
331 A total of nine logistic regression models were produced, one for each explanatory variable  
 332 and hydrologic class combination. Response variable was the presence (1) or the absence  
 333 (0) of a streambed. The area under the ROC (Receiver Operating Characteristic) curve was  
 334 used to evaluate model performance (Fawcett, 2006). The ROC curve plots the true positive

335 rate (1 minus omission) relative to the false positive rate (commission). This curve shows  
336 the performance of a given variable by determining the Area Under the Curve (AUC) and  
337 how the increase in the true positive rate will lead to an increase in the false positive rate.  
338 A model with a high AUC will provide a better balance between these two measurements  
339 and will produce better results. Thus, the AUC provides a measure of the ability of the  
340 individual variables to detect a streambed.

341 Next, four streambed models were compared to each other. Detection performance was  
342 calculated according to hydrological class and using Cohen's kappa, which is a measure of  
343 agreement between the true positive rate and the false positive rate (Cohen, 1960).

344 The first model examined was the GRHQ. An analysis distance of 6 m was used to compare  
345 properly the performance of the GRHQ with the other models. Two of the other three  
346 models corresponded to two different thresholds that were applied to the D8 variable,  
347 which is one of the most commonly used variables for generating stream networks. The  
348 first threshold was the median of the average drainage area of the channel heads surveyed  
349 in the field (referred to as Channel head; Fig. 3). The second threshold was the one that  
350 maximized Cohen's kappa for the variable D8 (referred to as Max Kappa). The last model  
351 that was compared is based on a supervised classification approach. This approach groups  
352 observations according to explanatory variables based on previously determined groups,  
353 also known as the response variable. In this case, the response variable was the presence  
354 or absence of a streambed. Classification And Regression Tree (CART) approach was used  
355 because of its ease of understanding the results and applying them over a wide area  
356 (Breiman et al., 1984). One tree was produced for each hydrologic class in order to describe  
357 the formation of headwater streams from homogeneous hydrologic processes.

358 The TPI and PROB variables were used for each hydrological class to produce trees. A  
 359 flow chart of the general method is shown in Figure 3. The depth and number of branches  
 360 in the classification trees have been pruned in order to prevent overfitting and it was  
 361 therefore not necessary to split the data into a training and a testing set (Fürnkranz, 1997).

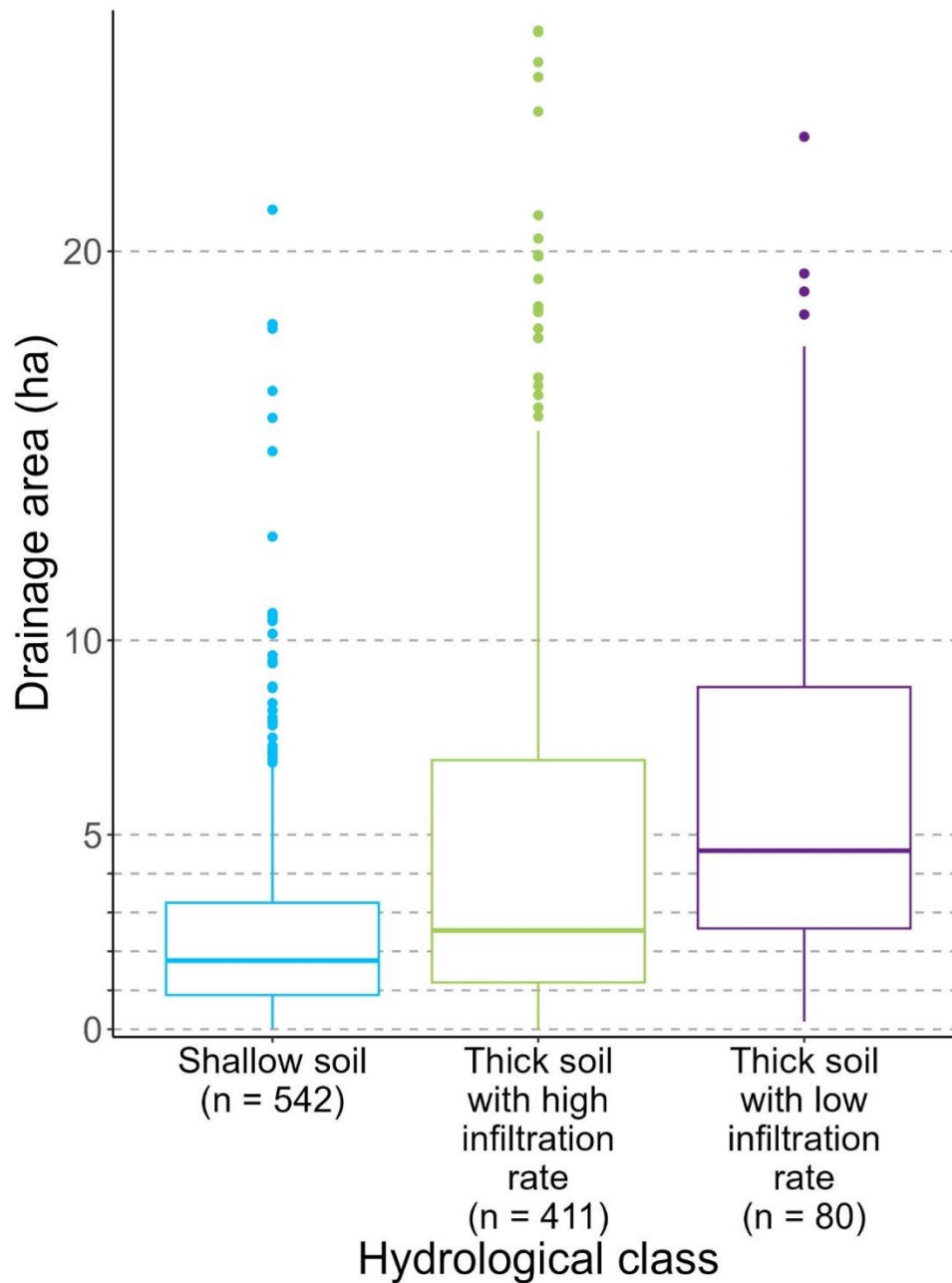


362  
 363 **Figure 3 :** Flowchart showing the methodology used to produce a raster describing the  
 364 presence of a streambed using classification trees [Color is not required for this figure.  
 365 2 column fitting figure.]

367 **4. Results**

368 A total of 464.7 km of streams were surveyed over an area of 161.5 km<sup>2</sup>. The positions of  
 369 1033 channel heads indicating the beginnings of streambeds were determined. The average  
 370 drainage areas of the channel heads are presented in Fig. 4 using whisker boxes according  
 371 to hydrological class. Figure 4 shows that for shallow soil, the average drainage area is less

372 variable than for thick soils. For thick soil with low infiltration rate, the average drainage  
373 area tends to be higher. Slope-drainage area curves and a visualization of different  
374 streambeds for each hydrological class are presented in Supplementary Materials.



375  
376 **Figure 4** : Distribution of mean drainage areas of channel heads according to hydrological  
377 class. Median values are shown. [Color is not required for this figure. Single column

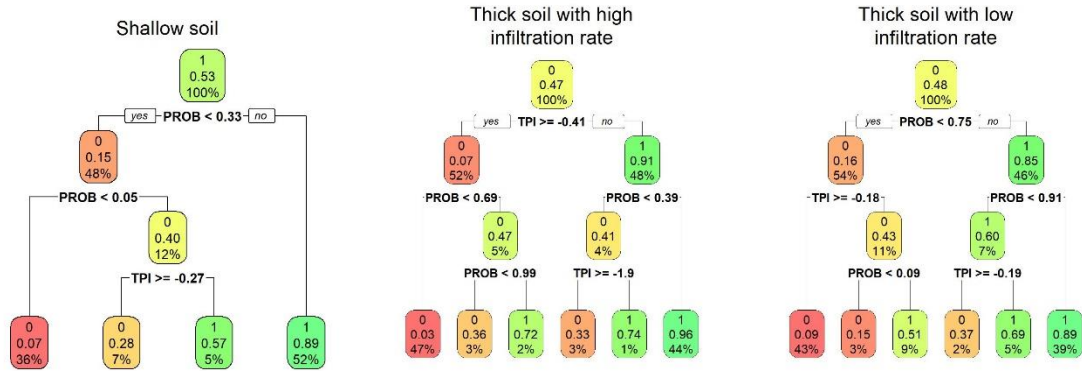
378 **fitting figure.]**

379

380 The analysis database contains a total of 40 354 positions describing streambeds (20 177  
381 with streambeds present and 20 177 with streambeds absent). A correlation matrix between  
382 the analysis variables showed that PROB is negatively correlated with TPI, with an R of -  
383 0.57. This variable therefore identifies where the water converges, which usually  
384 corresponds with the locations of incisions. The D8 variable was not correlated with other  
385 ones.

386 The classification trees according to hydrological class are presented in Fig. 5. The tree for  
387 shallow soil shows that when PROB exceeds a threshold of 0.33, a streambed is generally  
388 present. At the left side of the tree, when the PROB is very low, below 0.05, the streambed  
389 is generally absent. Otherwise, the TPI indicates whether a streambed is present or absent.  
390 For thick soil with a high infiltration rate, the incision indicated by the TPI first explains  
391 the presence of a streambed. When the incision is greater or equal to -0.41, indicating a  
392 small incision, PROB must be very high to indicate the presence of a streambed, at 0.99.  
393 When there is a larger incision, a lower value for PROB can identify the presence of a  
394 streambed. Thus, when the ground is relatively well incised with a TPI value smaller than  
395 -0.41, PROB only needs to be higher than 0.39 to detect a streambed. In thick soil with a  
396 low infiltration rate, PROB provides the initial information regarding the presence or  
397 absence of a streambed. Depending on the different PROB thresholds, TPI then determines  
398 the presence or absence of a streambed.

399



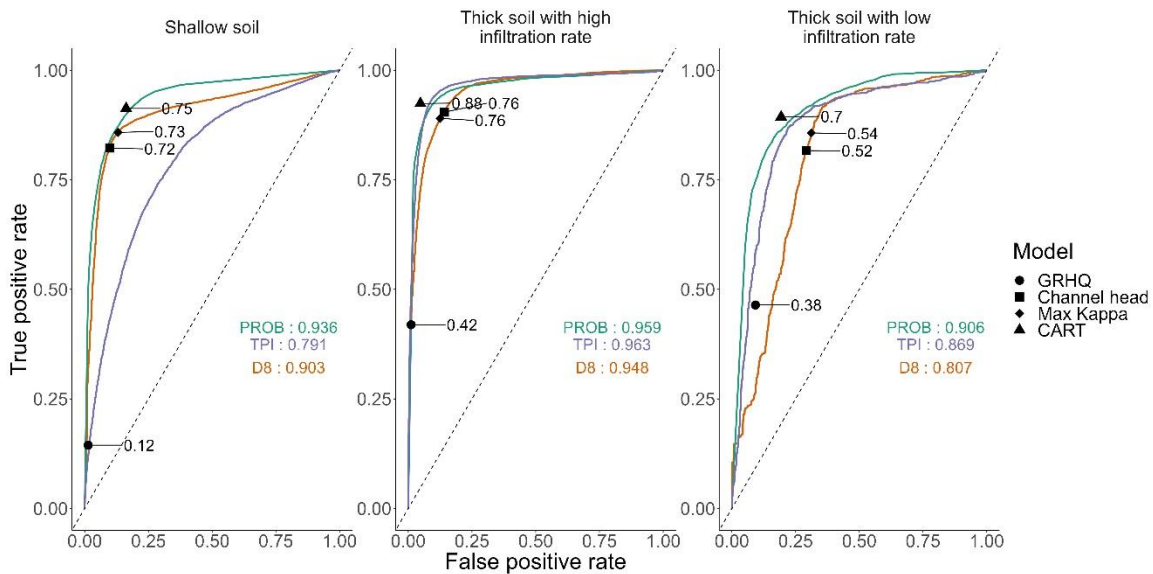
400

401 **Figure 5** : Classification trees to detect the presence of streambeds according to variables  
 402 D8, PROB and TPI and hydrological class. The colors red, orange, yellow and green  
 403 represent very low, low, medium, and high probability respectively. **[Color is not required**  
 404 **for this figure. 2 column fitting figure.]**

405

406 Figure 6 compares the AUC of individual variables, thus their potential to detect a  
 407 streambed. The performance of the four streambed models is also presented. This figure  
 408 shows that for the three hydrological classes, PROB performs more effectively than D8  
 409 when it comes to detecting streambeds. For thick soil classes, the incision variable TPI has  
 410 a higher AUC than D8. For shallow soil, the opposite is true. Compared to the other models,  
 411 the GRHQ has a very low true positive rate, meaning it omits many streams regardless of  
 412 the hydrologic class. However, the performance of GRHQ is higher for thick soil than for  
 413 shallow soil. For shallow soil, although the false positive rate is slightly lower for D8  
 414 thresholded with channel heads (Channel head), the Cohen's kappa of the classification  
 415 tree (CART) is still higher. The performance of the maximum Kappa of D8 (Max Kappa)  
 416 is still very similar to the one of the classification tree (CART). Figure 6 also shows that

417 for each class, the performance of the classification trees (CART) is in the upper left part  
 418 of the ROC curve of the variables used alone. This means that the combination of the  
 419 incision variable TPI with the PROB variable improves the detection of streambeds. For  
 420 thick soil with high infiltration rate, the two thresholding methods (Channel head and Max  
 421 Kappa) yielded similar performances, although they did not perform as well as the  
 422 classification tree (CART). The performance of the classification tree (CART) is also  
 423 higher than both D8 thresholding methods for thick soil with low infiltration rate. However,  
 424 the method using the maximum Kappa (Max Kappa) yields a higher rate of true positives  
 425 than the thresholding method using the channel heads (Channel head).  
 426



427  
 428 **Figure 6** : ROC curve and AUC values from the logistic regressions of the three variables  
 429 according to hydrological class. The performance of the streambed models using Cohen's  
 430 kappa is also presented. [Color is not required for this figure. 2 column fitting figure.]

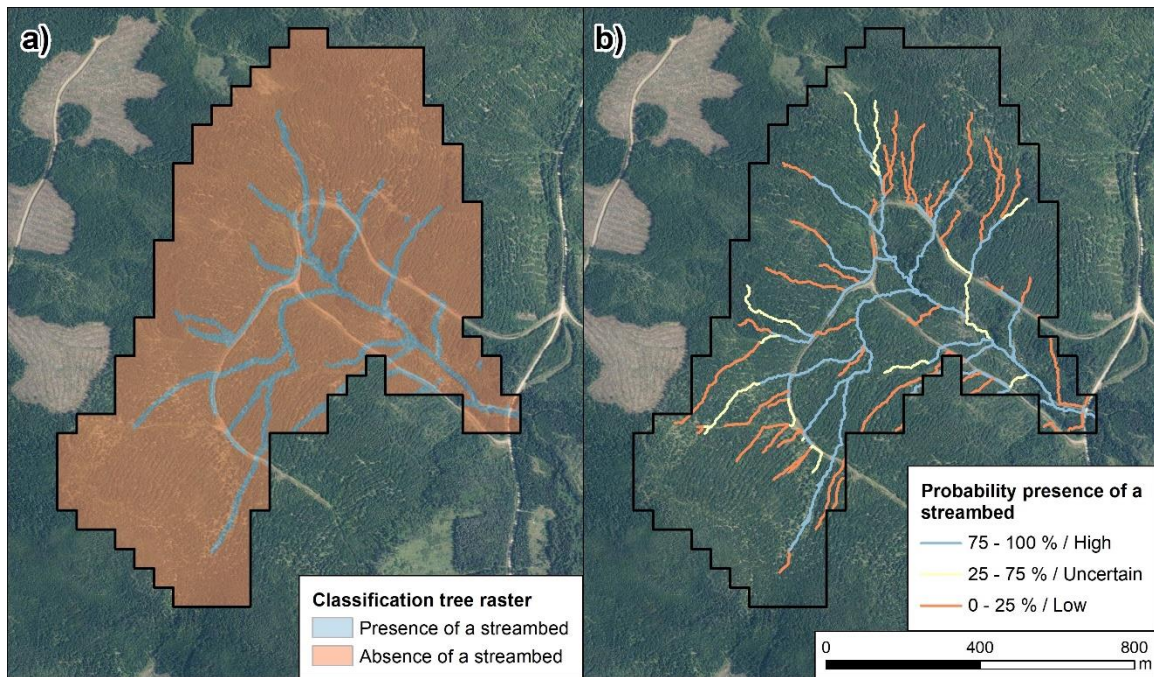
431

432 **5. Discussion**



433 The results suggest that the classification tree (CART) can detect streambeds more  
434 accurately than the other methods tested. By integrating different topographic indices and  
435 ground information such as Quaternary deposits, the detection of headwater streambeds is  
436 much more efficient in large watersheds, despite anthropization of the ground as  
437 agricultural fields that are sometimes present. In addition, as the results of the classification  
438 trees are rasters (Fig. 7a), they can be easily integrated within attribute table of a drainage  
439 network by calculating the mean using a zonal statistic to assess the probability presence  
440 of a streambed (Fig. 7b). This integration can be done without altering the course or  
441 thresholds of the hydrographic network. Each segment can therefore be truncated  
442 according to the presence or absence of the stream predicted by the model.

443



445 **Figure 7** : Classification tree that has been integrated into the segments of a hydrographic  
446 network to assess the probability presence of a streambed (b) (Aerial images from  
447 continuous imagery of the Government of Quebec; MRNF). [Color is not required for

448 **this figure. 1.5 column fitting figure.]**

449

450 The classification tree (CART) drastically increases the true positive rate compared to the  
451 GRHQ. This is because the GRHQ was based on aerial photographs that were primarily  
452 used to characterize vegetation and forest structure. Photointerpretation of these images  
453 did not allow for the detection of streambeds formed by local fluvial processes under the  
454 forest cover (Lessard, 2020). At most, photointerpretation enables the identification of  
455 valleys, for example, on thick soil (Montgomery and Dietrich, 1994). For this reason, the  
456 GRHQ omits fewer streams in thick soil than in shallow soil.

457 The PROB variable improved the detection of streambeds compared to the conventional  
458 use of only the D8 variable, since it has been thresholded to accurately match the lowest  
459 drainage areas of the channel heads. According to Fig. 4, the 1.5 ha threshold accounts for  
460 most of the channel heads. However, the drainage areas of the channel heads are generally  
461 higher for thick soil with low infiltration rate and could therefore lead to higher false  
462 positive rate. Most of the surveyed streams in this hydrologic class are located in the Abitibi  
463 Lowlands natural province. Furthermore, it is important to note that some of the drainage  
464 areas of the channel heads in shallow soil are smaller than 1.5 ha.

465 For the shallow soil hydrological class, the PROB variable improves streambed detection  
466 only when a false positive rate of at least 0.12 is specified. Figure 6 shows that for a false  
467 positive rate of 0.25, for example, PROB has a higher true positive rate than the D8  
468 variable. Streambeds that were not omitted with a PROB threshold greater than 0.12 were  
469 mostly small streams with highly variable positions due to the slightly upstream convex  
470 topography (Hengl et al., 2010). It seems that these streambed presence positions have very

471 low PROB values (48% of these positions have a probability below the 0.33 threshold used;  
472 Fig. 5). The 0.33 PROB threshold enabled a false positive rate that is much lower than  
473 0.25. In fact, the false positive rate was only 0.12. With this 0.33 threshold, the performance  
474 of PROB was almost identical to D8 (Fig. 6). To increase the true positive rate while using  
475 the PROB variable, the threshold could be decreased to allow the smallest streams to be  
476 identified. However, this modification would increase the false positive rate.

477 The poor performance of the TPI variable for shallow soil is due to the fact that the  
478 Quaternary deposits are generally thin and the slopes are frequently steep. The ground is  
479 therefore less prone to erosion and incision than for the other two hydrological classes  
480 (Jensen et al., 2018; Montgomery and Dietrich, 1994). Indeed, the parameters used to  
481 compute TPI do not enable the detection of small streambeds if they are not located in a  
482 valley or in a larger incision. Furthermore, the hydrological processes involved in this class  
483 are mostly surface flow and not subsurface flow. It is for this reason that D8 and PROB,  
484 which tend to be able to recreate surface flow quite precisely, are the best performing  
485 variables in this hydrological class (Julian et al., 2012; Wohl, 2018).

486 The incision variable TPI performed better in thick soil with high infiltration rate. This  
487 seems to be due to the fact that unlike shallow soil which are generally thin, infiltrative soil  
488 are thick and unconsolidated. Thus, the main hydrological process for this hydrological  
489 class is a subsurface process, where the water table plays an important role in the initiation  
490 of streambeds. Water infiltrates vertically into the permeable deposit and recharges the  
491 groundwater (Dunne and Black, 1970). The locations of the channel heads do not  
492 correspond to specific drainage areas that can be identified by flow accumulation variables,  
493 but rather to local incisions formed by gully processes where groundwater intersects the

494 ground surface (Dietrich and Dunne, 1993; Wohl, 2018). This process occurs where there  
495 is a significant change in slope or soil permeability. The emergence of water from the  
496 ground leads to progressive gullying that can be detected by incision variables  
497 (Montgomery and Dietrich, 1994). In this context, groundwater depth variables such as  
498 depth-to-water (DTW; (White et al., 2012)) could be used to explain the presence of  
499 streams in areas where a water table is present. It is important to mention that the DTW is  
500 very sensitive to parameterization and more research is needed for its proper use (Drolet,  
501 2020).

502 Streambeds were better detected using solely PROB instead of D8 for thick soil with low  
503 infiltration rate, which occur in territories where there is a high proportion of wetlands and  
504 gentle slopes. The PROB variable mostly reduces the number of commission cases. For  
505 example, in Fig. 6, PROB had a much lower false positive rate than D8 for the same true  
506 positive rate of 0.75. This large reduction in the false positive rate achieved with PROB  
507 reflects the ability of this variable to reproduce a diffuse flow on very flat or slightly convex  
508 terrains (Hengl et al., 2010). Indeed, in 78 % of cases, the positions that correspond to an  
509 absence of a streambed and that are corrected with PROB are wetlands. This is noteworthy  
510 because wetlands represent only 64 % of these positions in this hydrological class. Thus,  
511 the PROB variable, using uncertain DEM elevation information, can recreate more realistic  
512 behavior of the water, especially in thick soil with low infiltration rate. By using both  
513 PROB and TPI variables (Fig. 5), streambed detection for this hydrological class can be  
514 improved compared to the use of a single variable. Because the deposits are unconsolidated  
515 and the ground can be incised (Dietrich and Dunne, 1993), the classification tree is in the

516 upper left part of the ROC curve for the PROB variable as well as for the hydrological class  
517 with the high infiltration. The use of the TPI variable therefore provides an advantage.  
518 A limitation of the classification tree method is that the Quaternary deposit mapping is not  
519 accurate enough for all local hydrological issues. A visual inspection revealed some  
520 inconsistencies in the Quaternary deposit mapping within the same hydrological class.  
521 Another limitation is associated with the anthropization and straightening of natural  
522 streams. While a streambed is the result of a natural fluvial formation process that leads to  
523 ground erosion, an anthropic ditch is an artificial bed that is formed by mechanized digging.  
524 However, it is common for naturally formed streambeds to have been excavated and  
525 straightened in agricultural areas. In these cases, it becomes very difficult to distinguish a  
526 streambed from an anthropic ditch, even in the field. Excavation concentrates the flow of  
527 water in the artificial bed (Moussa et al., 2002). Thus, an area with previously no water  
528 flow could now be considered a streambed (Roelens et al., 2018). Automated detection  
529 methods are therefore likely to be much less reliable in these situations.  
530 We believe that the method described for calibrating the classification tree model is simple  
531 and robust enough to be applied in a different climatic and geomorphologic context with  
532 local data describing headwater streambeds. An accurate LiDAR derived headwater  
533 streambed mapping is a powerful tool for government and local organizations involved in  
534 water management and protection.

535

## 536 **6. Conclusion**

537 The classification tree method presented in this paper has improved the detection of  
538 headwater streambeds for different hydrological processes over large watersheds. Reliable

539 and consistent results were obtained by developing a comprehensive field database. The  
540 variable PROB, which describes the probability of occurrence of a streambed, was used to  
541 correct errors associated with the positioning of streambeds. This variable allowed for  
542 marginal corrections of streambeds in shallow soil, particularly when a high threshold was  
543 used. In order to more precisely explain where streams initiate in shallow soil, variables  
544 characterizing the composition of the upstream watershed such as the average upstream  
545 slope or the composition of deposits should be explored. The variable TPI, which  
546 characterized small-scale incisions, significantly improved the detection of streambeds in  
547 both thick soil hydrological classes when combined with the PROB variable. The small-  
548 scale incision variable worked better in soil with high infiltration rate and the probability  
549 of occurrence worked better in soil with low infiltration rate.

550 The increased complexity of the methods (inputs and parameterization) makes the  
551 optimizations more difficult for large and complex territories. The integration of all  
552 physiographic variables into a single model requires multiple iterations which leads to high  
553 complexity. Case studies could improve models by directly focusing on some of the  
554 identified limitations. It is also important to consider that the input data may sometimes be  
555 unreliable, such as those for the road network, culverts, Quaternary deposits, and land use.  
556 Thus, future developments, such as those integrating Quaternary deposits, will hardly be  
557 possible if the quality of the raw data remains unchanged. Visual interpretation of map  
558 products and verification by an expert with a good knowledge of the area is an essential  
559 step that should not be neglected under any circumstances.

560

561 **Author contribution**

562 Francis Lessard and Naïm Perreault contributed to the research project by providing  
563 expertise in methodology, software development, formal analysis, investigation, data  
564 curation, writing, and visualization. Their contributions encompassed various stages, from  
565 data collection and analysis to manuscript preparation.

566

567 Sylvain Jutras supervised the project, provided conceptual guidance, and played a role in  
568 writing and reviewing the manuscript. Additionally, Jutras secured funding for the project  
569 and managed administrative tasks related to its execution.

570

#### 571 **Competing interest**

572 The authors declare that they have no conflict of interest.

573

#### 574 **Acknowledgements**

575 The authors thank Quebec's Ministère de l'Environnement et de la Lutte contre les  
576 changements climatiques (MELCC) and Ministère des Forêts, de la Faune et des Parcs  
577 (MFFP), which funded this research project. This project would not have been possible  
578 without the exceptional collaboration of the MELCC's and MFFP's LiDAR mapping  
579 team, together with the many students and research associates who contributed to the  
580 numerous field surveys.

581

#### 582 **Data Availability**

583 Data and code can be found at [https://github.com/FraLessard/headwater\\_streambeds.git](https://github.com/FraLessard/headwater_streambeds.git),  
584 hosted at GitHub (Lessard and Perreault, 2023).

585

586 **References**

- 587 Alexander, R. B., Boyer, E. W., Smith, R. A., Schwarz, G. E., Moore, R. B.: The role of  
588 headwater streams in downstream water quality. *Journal of the American Water*  
589 *Resources Association*, 43(1), 41–59. [https://doi.org/10.1111/j.1752-](https://doi.org/10.1111/j.1752-1688.2007.00005.x)  
590 [1688.2007.00005.x](https://doi.org/10.1111/j.1752-1688.2007.00005.x), 2007.
- 591 Band, L. E.: Topographic Partition of Watersheds with Digital Elevation Models. *Water*  
592 *Resources Research*, 22(1), 15–24. <https://doi.org/10.1029/WR022i001p00015>,  
593 1986.
- 594 Blouin, J., and Berger, J.-P. : Guide de reconnaissance des types écologiques de la région  
595 écologique 5a – Plaine de l’Abitibi. Ministère des Ressources naturelles du Québec,  
596 Forêt Québec, Direction des inventaires forestiers, Division de la classification  
597 écologique et productivité des stations. 180 pp., 2002.
- 598 Blouin, J., and Berger, J.-P. : Guide de reconnaissance des types écologiques des régions  
599 écologiques 5e – Massif du lac Jacques-Cartier et 5f – Massif du mont Valin.  
600 Ministère des Ressources naturelles, de la Faune et des Parcs, Forêt Québec,  
601 Direction des inventaires forestiers, Division de la classification écologique et  
602 productivité des stations. 194 pp., 2004.
- 603 Breiman, L., Friedman, J. H., Olshen, R. A., & Stone, C. J.: *Classification And Regression*  
604 *Trees*. Routledge. <https://doi.org/10.1201/9781315139470>, 1984.
- 605 Cho, H. C., Clint Slatton, K., Cheung, S., & Hwang, S.: Stream detection for LiDAR digital  
606 elevation models from a forested area. *International Journal of Remote Sensing*,  
607 32(16), 4695–4721. <https://doi.org/10.1080/01431161.2010.484822>, 2011.



608 Cohen, J.: A Coefficient of Agreement for Nominal Scales. *Educational and Psychological*  
609 *Measurement*, 20(1), 37–46. <https://doi.org/10.1177/001316446002000104>, 1960.

610 Conrad, O., Bechtel, B., Bock, M., Dietrich, H., Fischer, E., Gerlitz, L., Wehberg, J.,  
611 Wichmann, V., & Böhner, J.: System for Automated Geoscientific Analyses  
612 (SAGA) v. 2.1.4. *Geoscientific Model Development*, 8(7), 1991–2007.  
613 <https://doi.org/10.5194/gmd-8-1991-2015>, 2015.

614 Couture, T.: Fish biodiversity and morphological quality in small agricultural streams of  
615 Montérégie, Québec. Master thesis. Department of Geography, Planning and  
616 Environment. Concordia University. 75 pp., 2023.

617 Creed, I. F., Lane, C. R., Serran, J. N., Alexander, L. C., Basu, N. B., Calhoun, A. J. K.,  
618 Christensen, J. R., Cohen, M. J., Craft, C., D’Amico, E., De Keyser, E., Fowler, L.,  
619 Golden, H. E., Jawitz, J. W., Kalla, P., Katherine Kirkman, L., Lang, M. W.,  
620 Leibowitz, S. G., Lewis, D. B., Marton, J., McLaughlin, D. L., Raanan-Kiperwas  
621 H., Rains M. C., Rains K. C., Smith, L.: Enhancing protection for vulnerable  
622 waters. *Nature Geoscience*, 10(11), 809–815. <https://doi.org/10.1038/NGEO3041>,  
623 2017.

624 Dietrich, W. E., and Dunne, T.: Sediment budget for a small catchment in mountainous  
625 terrain. *Z. Geomorph. N. F., Suppl. Bd.*, 29, 191–206., 1978.

626 Dietrich, W. E., and Dunne, T.: The Channel head. In: Beven K. and Kirkby M.J., Eds.,  
627 *Channel Network Hydrology*, Wiley, New York, 175-219., 1993.

628 Direction de l’expertise en biodiversité: Guide d’utilisation du Cadre écologique de  
629 référence du Québec (CERQ). Ministère du Développement durable, de  
630 l’Environnement et de la Lutte contre les changements climatiques (MDDELCC),

631 Québec. 24 pp., 2018.

632 Drolet, E. : Identification des zones de contrainte de drainage aux opérations forestières à  
633 l'aide des données lidar. Master thesis. Department of Wood and Forest Science.  
634 Université Laval. 62 pp., 2020.

635 Dunne, T., and Black, R. D.: An Experimental Investigation Runoff Production in  
636 Permeable Soils. *Water Resources Research*, 6(2), 478–490.  
637 <https://doi.org/10.1029/WR006i002p00478>, 1970.

638 Elmore, A. J., Julian, J. P., Guinn, S. M., & Fitzpatrick, M. C.: Potential Stream Density in  
639 Mid-Atlantic U.S. Watersheds. *PLoS ONE*, 8(8), e74819.  
640 <https://doi.org/10.1371/journal.pone.0074819>, 2013.

641 Estrada, D.: Smart Device / GNSS Receiver Assessment Study for Hydrographic. Office  
642 of the State Engineer Information Technology Services Bureau GIS (OSE GIS). 48  
643 pp., 2017.

644 Fairfield, J., and Leymarie, P.: Drainage Networks From Grid Digital Elevation Models.  
645 *Water Resources Research*, 27(5), 709-717. <https://doi.org/10.1029/90WR02658>,  
646 1991.

647 Fawcett, T.: An introduction to ROC analysis. *Pattern Recognition Letters*, 27(8), 861–  
648 874. <https://doi.org/10.1016/j.patrec.2005.10.010>, 2006.

649 Freeman, M. C., Pringle, C. M., & Jackson, C. R.: Hydrologic connectivity and the  
650 contribution of stream headwaters to ecological integrity at regional scales. *Journal*  
651 *of the American Water Resources Association*, 43(1), 5–14.  
652 <https://doi.org/10.1111/j.1752-1688.2007.00002.x>, 2007.

653 Freeman, T. G.: Calculating catchment area with divergent flow based on a regular grid.

654 Computers and Geosciences, 17(3), 413–422. <https://doi.org/10.1016/0098->  
655 [3004\(91\)90048-I](https://doi.org/10.1016/0098-3004(91)90048-I), 1991.

656 Fürnkranz, J.: Pruning Algorithms for Rule Learning. Machine Learning, 27, 139–172.  
657 <https://doi.org/10.1023/A:1007329424533>, 1997.

658 Gosselin, J.: Guide de reconnaissance des types écologiques des régions écologiques 3a –  
659 Collines de l’Outaouais et du Témiscamingue et 3b – Collines du lac Nominique.  
660 Ministère des Ressources naturelles du Québec, Forêt Québec, Direction des  
661 inventaires forestiers, Division de la classification écologique et de la productivité  
662 des stations. 188 pp., 2002.

663 Gosselin, J.: Guide de reconnaissance des types écologiques de la région écologique 3d -  
664 Coteaux des basses Appalaches. Ministère des Ressources naturelles et de la Faune,  
665 Direction des inventaires forestiers, Division de la classification écologique et  
666 productivité des stations. 186 pp., 2005a.

667 Gosselin, J.: Guides de reconnaissance des types écologiques de la région écologique 2b -  
668 Plaine du Saint-Laurent. Ministère des Ressources naturelles et de la Faune,  
669 Direction des inventaires forestiers, Division de la classification écologique et  
670 productivité des stations. 188 pp., 2005b.

671 Goulden, T., Hopkinson, C., Jamieson, R., and Sterling, S.: Sensitivity of watershed  
672 attributes to spatial resolution and interpolation method of LiDAR DEMs in three  
673 distinct landscapes. Water Resources Research, 50(3), 1908-1927.  
674 <https://doi.org/10.1002/2013WR013846>, 2014.

675 Guisan, A., Weiss, S. B., and Weiss, A. D.: GLM versus CCA spatial modeling of plant  
676 species distribution. Plant Ecology, 143(1), 107–122.

677 <https://doi.org/10.1023/A:1009841519580>, 1999.

678 Hafen, K. C., Blasch, K. W., Rea, A., Sando, R. and Gessler, P. E. : The Influence of  
679 Climate Variability on the Accuracy of NHD Perennial and Nonperennial Stream  
680 Classifications. *Journal of the American Water Resources Association*, 56(5), 903-  
681 916. <https://doi.org/10.1111/1752-1688.12871>, 2020.

682 Heine, R. A., Lant, C. L., and Sengupta, R. R.: Development and comparison of approaches  
683 for automated mapping of stream channel networks. *Annals of the Association of  
684 American Geographers*, 94(3), 477–490. [https://doi.org/10.1111/j.1467-  
685 8306.2004.00409.x](https://doi.org/10.1111/j.1467-8306.2004.00409.x), 2004.

686 Hengl, T., Heuvelink, G. B. M. M., and Van Loon, E. E.: On the uncertainty of stream  
687 networks derived from elevation data: the error propagation approach. *Hydrology  
688 and Earth System Sciences*, 14(7), 1153–1165. [https://doi.org/10.5194/hess-14-  
689 1153-2010](https://doi.org/10.5194/hess-14-1153-2010), 2010.

690 Henkle, J. E., Wohl, E., and Beckman, N.: Locations of channel heads in the semiarid  
691 Colorado Front Range, USA. *Geomorphology*, 129(3–4), 309–319.  
692 <https://doi.org/10.1016/j.geomorph.2011.02.026>, 2011.

693 Horton, B. Y. R. E.: Erosional development of streams and their drainage basins;  
694 Hydrophysical approach to quantitative morphology. *GSA Bulletin*, 56(3), 275–  
695 370. [https://doi.org/10.1130/0016-7606\(1945\)56\[275:EDOSAT\]2.0.CO;2](https://doi.org/10.1130/0016-7606(1945)56[275:EDOSAT]2.0.CO;2), 1945.

696 James, L. A., Hunt, K. J., Winter, S. W., James, L. A., and Hunt, K. J.: The LiDAR-side of  
697 Headwater Streams : Mapping Channel Networks with High-resolution  
698 Topographic Data. *Southeastern Geographer*, 50(4), 523–539.  
699 <https://doi.org/10.1353/sgo.2010.0009>, 2010.

700 James, L. A., Watson, D. G., and Hansen, W. F.: Using LiDAR data to map gullies and  
701 headwater streams under forest canopy: South Carolina, USA. *Catena*, 71(1), 132–  
702 144. <https://doi.org/10.1016/j.catena.2006.10.010>, 2007.

703 Jensen, C. K., McGuire, K. J., McLaughlin, D. L., and Scott, D. T.: Quantifying  
704 spatiotemporal variation in headwater stream length using flow intermittency  
705 sensors. *Environmental Monitoring and Assessment*, 191, 226.  
706 <https://doi.org/10.1007/s10661-019-7373-8>, 2019.

707 Jensen, C. K., McGuire, K. J., Shao, Y., and Andrew Dolloff, C.: Modeling wet headwater  
708 stream networks across multiple flow conditions in the Appalachian Highlands.  
709 *Earth Surface Processes and Landforms*, 43(13), 2762–2778.  
710 <https://doi.org/10.1002/esp.4431>, 2018.

711 Jenson, S. K., and Dominique, J. O.: Extracting topographic structure from digital elevation  
712 data for geographic information system analysis. *Photogrammetric Engineering*  
713 *and Remote Sensing*, 54(11), 1593–1600. 1988.

714 Julian, J. P., Elmore, A. J., and Guinn, S. M.: Channel head locations in forested watersheds  
715 across the mid-Atlantic United States: A physiographic analysis. *Geomorphology*,  
716 177–178, 194–203. <https://doi.org/10.1016/j.geomorph.2012.07.029>, 2012.

717 Leboeuf, A., and Pomerleau, I.: Projet d’acquisition de données par le capteur LiDAR à  
718 l’échelle provinciale : analyse des retombées et recommandations. Ministère des  
719 Forêts, de la Faune et des Parcs, Direction des inventaires forestiers. 15 pp., 2015.

720 Leopold, L. B., Wolman, M. G., and Miller, J. P.: *Fluvial Processes in Geomorphology*.  
721 San Francisco, California, W. H. Freeman and Company, 522 pp., 1964.

722 Lessard, F. Optimisation cartographique de l’hydrographie linéaire fine. Master thesis.

723 Department of Wood and Forest Science. Université Laval. 89 pp., 2020.

724 Lessard, F., Jutras, S., Perreault, N., and Guilbert, E.: Performance of automated  
725 geoprocessing methods for culvert detection in remote forest environments.  
726 Canadian Water Resources Journal,  
727 <https://doi.org/10.1080/07011784.2022.2160660>, 2023.

728 Li, R., Tang, Z., Li, X., and Winter, J. Drainage Structure Datasets and Effects on LiDAR-  
729 Derived Surface Flow Modeling. ISPRS International Journal of Geo-Information,  
730 2(4), 1136–1152. <https://doi.org/10.3390/ijgi2041136>, 2013.

731 Lindsay, J. B.: Sensitivity of channel mapping techniques to uncertainty in digital elevation  
732 data. International Journal of Geographical Information Science, 20(6), 669–692.  
733 <https://doi.org/10.1080/13658810600661433>, 2006.

734 Lindsay, J. B.: « Whitebox GAT: A Case Study in Geomorphometric Analysis ».  
735 Computers and Geosciences 95: 75-84.  
736 <https://doi.org/10.1016/j.cageo.2016.07.003>, 2016a.

737 Lindsay, J. B.: Efficient hybrid breaching-filling sink removal methods for flow path  
738 enforcement in digital elevation models. Hydrological Processes, 30(6), 846-857.  
739 <https://doi.org/10.1002/hyp.10648>, 2016b.

740 Lindsay, J. B., and Dhun, K.: Modelling surface drainage patterns in altered landscapes  
741 using LiDAR. International Journal of Geographical Information Science, 29(3),  
742 397–411. <https://doi.org/10.1080/13658816.2014.975715>, 2015.

743 Meyer, J. L., Strayer, D. L., Wallace, J. B., Eggert, S. L., Helfman, G. S., and Leonard, N.  
744 E.: The contribution of headwater streams to biodiversity in river networks. Journal  
745 of the American Water Resources Association, 43(1), 86–103.

746 <https://doi.org/10.1111/j.1752-1688.2007.00008.x>, 2007.

747 Ministère de l'Environnement et de la Lutte contre les changements climatiques  
748 (MELCC).: Normales climatiques du Québec 1981-2010. [data set].  
749 <https://www.environnement.gouv.qc.ca/climat/normales/>, 2022.

750 Montgomery, D. R., and Dietrich, W. E.: Channel Initiation and the Problem of Landscape  
751 Scale. *Science*, 255(5046), 826–830.  
752 <https://doi.org/10.1126/science.255.5046.826>, 1992.

753 Montgomery, D. R., and Dietrich, W. E.: Landscape dissection and drainage area-slope  
754 thresholds. In: Kirkby, M.J. (Ed.), *Process Models and Theoretical  
755 Geomorphology*. John Wiley and Sons, 221–246. 1994.

756 Montgomery, D. R., and Foufoula-Georgiou, E.: Channel Network Source Representation  
757 Using Digital Elevation Models. *Water Resources Research*, 29(12), 3925–3934.  
758 <https://doi.org/10.1029/93WR02463>, 1993.

759 Moussa, R., Voltz, M., and Andrieux, P.: Effects of the spatial organization of agricultural  
760 management on the hydrological behaviour of a farmed catchment during flood  
761 events. *Hydrological Processes*, 16(2), 393–412. <https://doi.org/10.1002/hyp.333>,  
762 2002.

763 Murphy, P. N. C., Ogilvie, J. and Arp, P. A.: Topographic modelling of soil moisture  
764 conditions: a comparison and verification of two models. *European Journal of Soil  
765 Science*, 60(1), 94-109. <https://doi.org/10.1111/j.1365-2389.2008.01094.x>, 2009.

766 Murphy, P. N. C., Ogilvie, J., Meng, F.-R. R., and Arp, P. A.: Stream network modelling  
767 using lidar and photogrammetric digital elevation models: a comparison and field  
768 verification. *Hydrological Processes*, 22(12), 1747-1754.

769 <https://doi.org/10.1002/hyp.6770>, 2008.

770 O’Callaghan, J. F., and Mark, D. M.: The extraction of drainage networks from digital  
771 elevation data. *Computer Vision, Graphics, and Image Processing*, 28(3), 323–344.  
772 [https://doi.org/10.1016/S0734-189X\(84\)80011-0](https://doi.org/10.1016/S0734-189X(84)80011-0), 1984.

773 O’Neil, G., and Shortridge, A.: Quantifying local flow direction uncertainty. *International  
774 Journal of Geographical Information Science*, 27(7), 1292–1311.  
775 <https://doi.org/10.1080/13658816.2012.719627>, 2013

776 Passalacqua, P., Belmont, P., and Fofoula-Georgiou, E.: Automatic geomorphic feature  
777 extraction from lidar in flat and engineered landscapes. *Water Resources Research*,  
778 48(3), 1–18. <https://doi.org/10.1029/2011WR010958>, 2012.

779 Persendt, F. C., and Gomez, C.: Assessment of drainage network extractions in a low-relief  
780 area of the Cuvelai Basin (Namibia) from multiple sources: LiDAR, topographic  
781 maps, and digital aerial orthophotographs. *Geomorphology*, 260, 32–50.  
782 <https://doi.org/10.1016/j.geomorph.2015.06.047>, 2016.

783 Peucker, T. K., and Douglas, D. H.: Detection of Surface-Specific Points by Local Parallel  
784 Processing of Discrete Terrain Elevation Data. *Computer Graphics and Image  
785 Processing*, 4(4), 375–387. [https://doi.org/10.1016/0146-664x\(75\)90005-2](https://doi.org/10.1016/0146-664x(75)90005-2), 1975.

786 Richardson, M. and Millard, K.: *Geomorphic and Biophysical Characterization of Wetland  
787 Ecosystems with Airborne LiDAR Concepts, Methods, and a Case Study. High  
788 Spatial Resolution Remote Sensing 1<sup>st</sup> Edition*, CRC Press, 39 pp. ISBN:  
789 9780429470196, 2018.

790 Roelens, J., Rosier, I., Dondeyne, S., Van Orshoven, J., and Diels, J.: Extracting drainage  
791 networks and their connectivity using LiDAR data. *Hydrological Processes*, 32(8),



792 1026–1037. <https://doi.org/10.1002/hyp.11472>, 2018.

793 Sanders, K. E., Smiley Jr., P. C., Gillespie, R. B., King, K. W., Smith, D. R., and Pappas,  
794 E. A.: Conservation implications of fish–habitat relationships in channelized  
795 agricultural headwater streams. *Journal of Environmental Quality*, 49(6), 1585-  
796 1598. <https://doi.org/10.1002/jeq2.20137>, 2020.

797 Saucier, J.-P., Berger, J.-P., D’Avignon, H., and Racine, P.: Le point d’observation  
798 écologique. Ministère des Ressources naturelles, Direction de la gestion des stocks  
799 forestiers, Service des inventaires forestiers. 116 pp., 1994.

800 Schwanghart, W., and Heckmann, T.: Fuzzy delineation of drainage basins through  
801 probabilistic interpretation of diverging flow algorithms. *Environmental Modelling  
802 and Software*, 33, 106–113. <https://doi.org/10.1016/j.envsoft.2012.01.016>, 2012.

803 St-Hilaire, A., Duchesne, S., and Rousseau, A. N.: Floods and water quality in Canada: A  
804 review of the interactions with urbanization, agriculture and forestry. *Canadian  
805 Water Resources Journal*, 41(1–2), 273–287.  
806 <https://doi.org/10.1080/07011784.2015.1010181>, 2016.

807 Tribe, A.: Automated recognition of valley lines and drainage networks from grid digital  
808 elevation models: a review and a new method. *Journal of Hydrology*, 139(1–4),  
809 263–293. [https://doi.org/10.1016/0022-1694\(92\)90206-B](https://doi.org/10.1016/0022-1694(92)90206-B), 1992.

810 Tucker, G. E., and Slingerland, R.: Predicting sediment flux from fold and thrust belts.  
811 *Basin Research*, 8(3), 329–349. <https://doi.org/10.1046/j.1365-2117.1996.00238.x>,  
812 1996.

813 Van Meerveld, H. J. I., Kirchner, J. W., Vis, M. J. P., Assendelft, R. S., and Seibert, J.:  
814 Expansion and contraction of the flowing stream network changes hillslope

815 flowpath lengths and the shape of the travel time distribution. *Hydrology and Earth*  
816 *System Sciences*, 23(11), 4825-4834. <https://doi.org/10.5194/hess-23-4825-2019>,  
817 2019.

818 Wechsler, S. P.: Uncertainties associated with digital elevation models for hydrologic  
819 applications: a review. *Hydrology and Earth System Sciences*, 11(4), 1481–1500.  
820 <https://doi.org/10.5194/hess-11-1481-2007>, 2007.

821 Weiss, A.: Topographic position and landforms analysis. Poster Presentation, ESRI User  
822 Conference, San Diego, California. USA. 2001.

823 White, B., Ogilvie, J., Campbell, D. M. H., Hiltz, D., Gauthier, B., Chisholm, H. K. H.,  
824 Wen, H. K., Murphy, P. N. C., and Arp, P. A.: Using the Cartographic Depth-to-  
825 Water Index to Locate Small Streams and Associated Wet Areas across  
826 Landscapes. *Canadian Water Resources Journal*, 37(4), 333–347.  
827 <https://doi.org/10.4296/cwrj2011-909>, 2012.

828 Wohl, E.: The challenges of channel heads. *Earth-Science Reviews*, 185, 649–664.  
829 <https://doi.org/10.1016/j.earscirev.2018.07.008>, 2018.

830 Wu, J., Liu, H., Wang, Z., Ye, L., Li, M., Peng, Y., Zhang, C., and Zhou, H.: Channel head  
831 extraction based on fuzzy unsupervised machine learning method. *Geomorphology*,  
832 391, 107888. <https://doi.org/10.1016/j.geomorph.2021.107888>, 2021.

833 Wulder, M. A., Bater, C. W., Coops, N. C., Hilker, T., White, J. C.: The role of LiDAR in  
834 sustainable forest management. *Forestry Chronicle*, 84(6), 807–826.  
835 <https://doi.org/10.5558/tfc84807-6>, 2008.